DEPARTMENT OF MECHANICAL ENGINEERING & MECHANICS
COLLEGE OF ENGINEERING & TECHNOLOGY
OLD DOMINION UNIVERSITY
NORFOLK, VIRGINIA 23529

VISCOUS EFFECTS ON A VORTEX WAKE IN GROUND EFFECT

By

Z. Zheng, Graduate Research Assistant

and

Robert L. Ash, Principal Investigator

Final Report
For the period ended May 31, 1991

Prepared for
National Aeronautics and Space Administration
Langley Research Center
Hampton, Virginia 23665

Under
Research Grant NAG-1-987
George C. Greene, Technical Monitor
FAD-Flight Research Branch

Submitted by the
Old Dominion University Research Foundation
P.O. Box 6369
Norfolk, Virginia 23508-0369

June 1992

Viscous Effects on a Vortex Wake in Ground Effect

by

Z. Zheng* and R. L. Ash†

Abstract

Wake vortex trajectories and strengths are altered radically by interactions with the ground plane. Prediction of vortex strength and location is especially important in the vicinity of airports. Simple potential flow methods have been found to yield reasonable estimates of vortex descent rates in an otherwise quiescent ambient background, but those techniques cannot be adjusted for more realistic ambient conditions and they fail to provide satisfactory estimates of ground-coupled behavior. The authors have been involved in a systematic study concerned with including viscous effects in a wake-vortex system which is near the ground plane. The study has employed numerical solutions to the Navier-Stokes equations, as well as perturbation techniques to study ground coupling with a descending vortex pair.

Results of a two-dimensional, unsteady numerical-theoretical study are presented in this paper. A time-based perturbation procedure has been developed which permits the use of analytical solutions to an inner and outer flow domain for the initial flow field. Predictions have been compared with previously reported laminar experimental results. In addition, the influence of stratification and turbulence on vortex behavior near the ground plane has been studied.

---

* Graduate Research Assistant

† Professor and Chairman, Mechanical Engineering and Mechanics Department,
Old Dominion University, Norfolk, VA 23529-0247
Tel. (804) 683-3720, Fax (804) 683-5344

Introduction

It is known that aircraft trailing vortex wakes can cause serious loss of control when following aircraft encounter them. The hazard is more severe near the ground because of the limited time and space available to maneuver the aircraft. Therefore, prediction of wake vortex trajectories and strengths is especially important for effective airport flight control. The work reported here has been focused on the viscous interaction between vortex wakes and the ground plane.

Potential theory representation of a pair of counter-rotating vortex filaments above an infinite plane yields reasonable estimates of wake vortex descent rates in an otherwise quiescent atmosphere, when the wake is sufficiently far from the ground (Saffman 1979). By assuming the vortices could be treated as small core sized vorticity spots above a very thin ground boundary-layer, Liu and Ting (1987) determined that away from the small cores and the thin boundary-layer region, the flowfield obeyed the Euler equations. From that perspective, it is very inefficient and expensive to study the trailing vortex problem using Navier-Stokes solvers for the entire flow field. However, the methods of Liu and Ting (1987) are only valid when the vortical spot is sufficiently far away from the ground relative to the core size, so that vortex-core interactions with the ground-plane boundary layer can be neglected. Hence, Euler equations can be used to model large portions of the computational domain, but that region must be adjusted continuously near the ground plane.

It should be stated that without ground effect, even in more realistic atmospheric conditions, an approximate model developed by Greene (1986) demonstrated surprisingly good agreement with experimental data. That method was based upon empirical engineering approximations. But from the authors' experience, the extension required to include ground effects was not compatible with Greene's model.

Experiments to establish the features of the flowfield induced by a single vortex near the ground were carried out by Harvey and Perry (1971) in a low-speed wind tunnel. The primary objective of those experiments was to explain the cause of the vortex rebound phenomenon which is considered to be a significant feature of the ground effect and which can influence terminal flight conditions. They inferred that rebound was caused by separation of the ground boundary-layer flow underneath the vortex. They argued that boundary-layer separation produces a secondary vortex whose development makes the primary vortex rise. Later Barker and Crow (1977) observed rebound for a vortex pair, generated in water, approaching either a free upper surface or a rigid horizontal plane immersed in the water. They asserted that the phenomenon could be attributed to the effect of finite vortex core size. Recently, experiments were designed by Liu and Srnsky (1990) to minimize the sidewall effects that can mask the ground effects. From their dye visualization results in water, they identified the emergence of secondary, counter-rotating vortices outboard from the vortex wake near ground level. They determined that as soon as the secondary vortex began to form, rebound of the main vortex was initiated. Specifically, the primary and secondary vortices form a vortex pair that moves upward. Those results have confirmed essentially the scenario of secondary vortex generation suggested by Harvey and Perry (1971).

Many theoretical studies of a vortex pair in ground effect have been reported during the last two decades. Research reported by Bilanin, Teske and Hirsh (1978), Saffman (1979) and Peace and Riley (1983) disagreed with the finite core size hypothesis of Barker and Crow (1977). Saffman (1979) showed, within the framework of inviscid theory, that it was not possible to explain the rebound phenomenon by finite core size and that the wallward velocity component cannot change sign. Navier-Stokes computational results for a trailing vortex pair near the ground were performed by Bilanin, Teske and Hirsh (1978) for both laminar and turbulent conditions. They demonstrated that the rebound did not occur unless the viscous, no-slip boundary condition

was applied. One of the important conclusions drawn by them was that the proximity of a ground plane reduces the vortex hazard by scrubbing. That is, the vortex pair separates or spreads and interacts viscously with the ground thereby reducing its strength more rapidly. A numerical study of the effects of stratification and wind shear on the evolution of aircraft wake vortices near the ground was also included in the report by Delisi, Robins and Fraser (1987), who found that both effects reduce the extent of vortex rebound. As they stated, turbulence was not included formally in their computational model. But some *ad hoc* small scale damping was added to the equations included in the numerical model. They thought this simple "turbulence model" was adequate to predict vortex migration. In addition, a mixed no-slip/slip boundary condition was invoked on the ground plane which needed an empirical adjustment for different flow cases.

In the work which follows, a two-dimensional, unsteady numerical-theoretical study will be reported. A time-dependent double series, asymptotic expansion in terms of Reynolds number and time has been used for the initial flow field. The computational domain and grid spacing have been chosen carefully to avoid using approximate boundary conditions and to get proper resolution. Subsequently, the influences of stratification and turbulence on vortex behavior near the ground plane have been shown.

Computational Approach

An unsteady vorticity, stream-function formulation has been used in the numerical calculations. Invoking symmetry of the vortex pair permits the computations to be restricted to the first quadrant ($0 \leq x < \infty,\ 0 \leq y < \infty$). The system of equations were made dimensionless using the initial vortex half-span, s_0, as the characteristic length and the initial circulation, Γ_0, along with the fluid density, ρ_0, to formulate the other dimensionless variables. The characteristic flow Reynolds number is $Re = \Gamma_0/\nu_0$, where ν_0 is the kinematic viscosity. Characteristic velocity,

time and pressure are given by Γ_0/s_0, s_0^2/Γ_0 and $\rho_0\Gamma_0^2/s_0^2$, respectively. Since there is only one component of vorticity, ζ, the governing vorticity and stream-function (ψ) equations are:

$$\frac{\partial \zeta}{\partial t} + \left(\vec{u}\cdot\vec{\nabla}\right)\zeta = \frac{1}{Re}\nabla^2\zeta \tag{1}$$

and

$$\nabla^2\psi = -\zeta \tag{2}$$

respectively. Here

$$\vec{u} = u\vec{i} + v\vec{j} \tag{3}$$

and

$$\zeta = \frac{\partial v}{\partial x} - \frac{\partial u}{\partial y}, \quad \text{with} \quad u = \frac{\partial \psi}{\partial y}, \quad \text{and} \quad v = -\frac{\partial \psi}{\partial x} \ . \tag{4}$$

The coordinate system is shown in Figure 1.

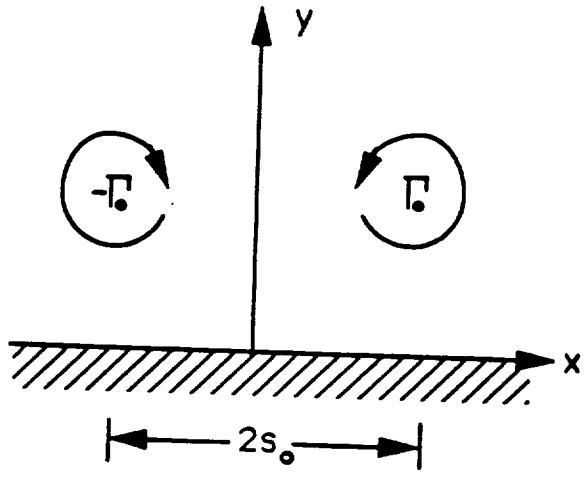

Figure 1. Coordinate system employed in this study

Since the flow is for the most part inviscid, with an unsteady, viscous ground-plane boundary layer and a small viscous vortex core region, problems were encountered in starting the numerical calculations. The initial velocity field problem has been addressed previously by Peace and Riley (1983), but they used a single series expansion in time, scaled by Reynolds number (t/R_e), to start their asymptotic solution. Limitations of the single series expansion for unsteady boundary-layer flows have been discussed by Nam (1990). Considerable effort was devoted to developing an appropriate initial velocity field which accommodated the ground effect region in the numerical simulation without producing non-physical, numerical start-up transients. A forthcoming contractor report (Ash and Zheng 1991) contains a more detailed derivation of the asymptotic expansion formulations, but the essential features of the approach are developed below. In addition, the computational domain transformation procedure and boundary condition specifications are discussed.

Flow Field Initialization

Since a goal of this study was to extend the Reynolds number range over which vortex-ground plane interactions could be modeled, viscous effects were anticipated in both the vortex core and boundary layer regions long before any interactions between the vortex core(s) and boundary layer occurred. Furthermore, a fine numerical grid was required for both the vortex region, including its path of descent, and the ground-plane boundary layer. Both requirements demanded an initial velocity field which was free of anomalous velocity gradients.

The Oseen (1911) vortex is an exact solution to the Navier-Stokes equations for the diffusion of a vortex filament into a viscous region of infinite extent. For any time greater than zero, the Oseen vortex includes viscosity, while at $t = 0$, it is an inviscid point vortex. Hence, placing a pair of those vortices at $\pm x_0$, y_0 at $t = 0$, is equivalent to placing a pair of potential vortices at those locations, but then allowing viscous effects to occur immediately after placement. Oseen

vortex solutions do not include either non-linear coupling of the vortex pair or the viscous influence of a ground plane. Adding a mirror image pair of Oseen vortices (at $\pm x_0,\ -y_0$) can be used to initiate a ground plane interaction. Since those vortices proceed immediately to viscous flows, they appear to be a more realistic starting flow than that of a pair of potential vortices in any practical numerical grid. Hence, analytic perturbation methods can be used to predict the flow during the initial time interval when local velocity gradients create severe problems for numerical techniques.

In the ground plane boundary-layer region, the initial stream-function $\psi(x, y, t)$ is assumed to take the form:

$$\psi(x, y, t) = 2\epsilon[\psi_1(x, \eta, t) + \epsilon\psi_2(x, \eta, t) + \cdots] \tag{5}$$

where $\epsilon = \sqrt{t/Re}$ and $\eta = y/2\epsilon$, with

$$\psi_i(x, \eta, t) = \sum_{p=0}^{\infty} t^p \phi_p^i(x, \eta, t) \tag{6}$$

This stream-function must satisfy the no-slip boundary conditions.

In the outer flow, it is assumed that the stream-function can be represented initially by

$$\Psi(x, y, t) = \Psi_0(x, y, t) + \epsilon\Psi_1(x, y, t) + \cdots \tag{7}$$

This stream-function must satisfy the initial potential vortex requirements of both a symmetry plane and a ground plane. Application of the two-dimensional, incompressible Navier-Stokes equations to the two stream-function series and matching the expansions using van Dyke (1976) type matching procedures yields

$$\psi = 2\epsilon(\psi_1 + \epsilon\psi_2) + O[\epsilon^3] \tag{8}$$

where

$$\psi_1 = U_0 f_{01} + t\left(\frac{\partial U_0}{\partial t} f_{11} + U_0 \frac{\partial U_0}{\partial x} f_{12}\right) + O[t^2] \tag{9}$$

$$\psi_2 = U_1 g_{01} + t\left(\frac{\partial U_1}{\partial t} g_{11} + U_0 \frac{\partial U_1}{\partial x} g_{12} + U_1 \frac{\partial U_0}{\partial x} g_{13}\right) + O\left[t^2\right] \tag{10}$$

$$f_{01} = \eta\ erf(\eta) + \frac{1}{\pi^{1/2}} e^{-\eta^2} - \frac{1}{\pi^{1/2}} \tag{11}$$

$$f_{11} = \frac{1}{3\pi^{1/2}}\left(1 - e^{-\eta^2}\right) - \frac{2}{3}\eta^3 erfc(\eta) + \frac{2}{3\pi^{1/2}}\eta^2 e^{-\eta^2} \tag{12}$$

$$\begin{aligned} f_{12} = &- \frac{11}{6\pi^{1/2}}\left(1 - e^{-\eta^2} erfc(\eta)\right) + \frac{8}{3\sqrt{2}\pi^{1/2}} erf\left(\sqrt{2}\eta\right) - \frac{1}{3}\left(2 + \frac{4}{3\pi}\right)\eta^3 erfc(\eta) \\ &- \frac{2}{3\pi^{1/2}}\eta^2 e^{-\eta^2} erfc(\eta) + \frac{1}{3\pi}\eta e^{-2\eta^2} - \frac{1}{2}\eta\ erfc^3(\eta) + \left(\frac{3}{2\pi^{1/2}} - \frac{4}{9\pi^{3/2}}\right)\left(1 - e^{-\eta^2}\right) \\ &+ \left(\frac{1}{2} - \frac{2}{3\pi}\right)\eta erfc(\eta) - \frac{2}{3\pi^{1/2}} erf(\eta) + \left(\frac{1}{\pi^{1/2}} + \frac{4}{9\pi^{3/2}}\right)\eta^2 e^{-\eta^2} \end{aligned} \tag{13}$$

$$g_{01} = \eta + \frac{1}{2}\pi^{1/2}\eta^2 erfc(\eta) - \frac{1}{2}\eta e^{-\eta^2} - \frac{1}{4}\pi^{1/2} erf(\eta) \tag{14}$$

$$g_{11} = \frac{\pi^{1/2}}{4}(\eta^3 + \eta^4) erfc(\eta) + \frac{1}{2}\int_o^\eta (-\eta^2 + \eta^4) e^{-\eta^2} d\eta \tag{15}$$

$$\begin{aligned} g_{12} = &\int_0^\eta \left\{ \frac{7}{6}\pi^{1/2}\left(\eta + \frac{2}{3}\eta^3\right) - \frac{\pi^{1/2}}{4}\left[\left(\eta + \frac{2}{3}\eta^3\right) erf(\eta) + \frac{2}{3\pi^{1/2}}(1 + \eta^2) e^{-\eta^2}\right] \right. \\ &+ \pi^{1/2}\left(-\frac{1}{2}\eta - \eta^3\right)(erf(\eta))^2 + \left(-\frac{1}{2} - 2\eta^2\right) e^{-\eta^2} erf(\eta) - \frac{1}{8}\eta e^{-2\eta^2} \\ &\left. - \pi^{1/2}\eta\ erf(\eta) - \frac{2}{3} erf(\eta) + \frac{2}{3} - \frac{1}{2} e^{-\eta^2} \right\} d\eta \end{aligned} \tag{16}$$

$$g_{13} = \frac{3}{8}\pi^{1/2}\left(\eta^2 + \frac{1}{3}\eta^4\right) erfc(\eta) + \frac{1}{2}\int_0^\eta \left(\eta^2 + \frac{1}{3}\eta^4\right) e^{-\eta^2} d\eta \tag{17}$$

It is noted that $U_0(x,t)$ and $U_1(x,t)$ are the outer flow representations of the vortices along the ground plane ($y = 0$). These solutions are restricted to small times and are given by

$$U_0(x,t) = \frac{4}{\pi} \frac{y_0 x}{\left[(x-1)^2 + y_0^2\right]\left[(x+1)^2 + y_0^2\right]} \tag{18}$$

and

$$U_1(x,t) = \frac{2}{\pi^{3/2}} \int_0^\infty \left. \frac{\partial U_0}{\partial x} \right|_{x=\xi} \frac{d\xi}{x-\xi} \tag{19}$$

which are the same forms used by Peace and Riley (1983).

In effect, four Oseen vortex solutions, with Cartesian velocity components given by

$$\begin{aligned} U_c(x,y,t) = {} & (y-y_0)[\Phi(x,y,t;-1,y_0) - \Phi(x,y,t;1,y_0)] \\ & + (y+y_0)[\Phi(x,y,t;1,-y_0) - \Phi(x,y,t;-1,-y_0)] \end{aligned} \tag{20}$$

and

$$\begin{aligned} V_c(x,y,t) = {} & (x-1)[\Phi(x,y,t;1,y_0) - \Phi(x,y,t;1,-y_0)] \\ & + (x+1)[\Phi(x,y,t;-1,-y_0) - \Phi(x,y,t;-1,y_0)] \end{aligned} \tag{21}$$

where

$$\Phi(x,y,t;\alpha,\beta) = \frac{1}{2\pi} \frac{1 - e^{-Re\left[(x-\alpha)^2 + (y-\beta)^2\right]/4t}}{(x-\alpha)^2 + (y-\beta)^2} \tag{22}$$

have been employed in the outer flow, in the vicinity of $x = 1$, $y = y_0$. Again, these functions are restricted to small times, where they do not alter the asymptotic matching conditions.

To summarize, the asymptotically generated velocity field, which constitutes the initial velocity distribution in the numerical scheme, is a combination of solutions (7), (8), (20) and (21). Small values of time, compared to the Reynolds number, have been employed. The asymptotic solution time level selected to generate the initial velocity field depended on the circulation Reynolds number, but it was the maximum time allowable by the finite term approximations

to the infinite series expansions. The asymptotic solutions were thus used to produce an initial velocity field whose local gradients could be handled by the numerical grid, but whose series representations did not represent a significant amount of computational overhead.

Domain Transformation and Boundary Conditions

A moving grid was considered for this study but was discarded subsequently, due to the complexity of the vortex trajectory in ground effect and to uncertainty in the viscous zones requiring fine grid resolution. It was deemed more reasonable to pack grid points adjacent to the symmetry- and ground-planes and allow the vortex system to move with respect to the grid. This was possible because the nominal regions where viscous effects occurred were known to a first order approximation. It is noted further that the elliptic character of the incompressible flow field mandates enforcing the boundary conditions at the infinite limits of x and y or alternatively developing rigorous boundary condition approximations within a finite domain.

Bilanin et al (1977) and Ting (1983) studied the far field boundary condition problem. They used the far field expansions of Poisson integrals which could be employed in a finite subdomain of an unbounded fluid. The exponential decay laws for vorticity distributions were required for the convergence of the far field expansions (Ting 1983). The expansions were developed further by Ting (1983) using integral invariants. Unfortunately, neither the decay laws nor the integral invariants exist when a no-slip boundary is present because the vorticity distribution in the viscous ground-plane boundary layer cannot be estimated *a priori*. Here a coordinate mapping has been used, employing a simple exponential transformation which yields densely packed grid points near the ground plane and stretches the grid as the infinite limits are approached. The mapping

$$X = a\left(1 - e^{-bx}\right)$$
$$Y = c\left(1 - e^{-dy}\right) \tag{23}$$

transforms $0 \leq x < \infty,\ 0 \leq y < \infty$ into the finite domain $0 \leq X < a,\ 0 \leq Y < c$. The corresponding spacing intervals are

$$\Delta X \approx abe^{-bx}\Delta x$$

$$\Delta Y \approx cde^{-dy}\Delta y \tag{24}$$

Hence the boundary-layer and vortex core resolution can be controlled by adjusting the arbitrary constants $a,\ b,\ c$ and d.

Since the ground plane spacing is compressed automatically via the coordinate mapping, resolution requirements are more severe in the far field. In addition, vortex core resolution in the vertical direction is most sensitive at start-up ($y = y_0$), while horizontal resolution is least accurate at the end of the numerical simulation (when the vortex core is at the greatest horizontal distance from the symmetry plane) — say x_l. Since the vortex dilates as time increases, selecting an appropriate grid spacing initially produces a conservative spacing level at later times.

As an example, if the initial vortex core radius is $r_c = 0.2$, then we would require that $\Delta y_{\max} = 0.02\ (= r_c/10)$ at y_0, and that $\Delta x_{\max} = 0.1\ (= r_c/2)$ at x_l. The $\Delta x_{\max}$ spacing will be more compact relative to the vortex core due to dilation beginning from $t = 0$. However, the spacing interval is given by:

$$\Delta X \leq 0.1\ abe^{-bx_l}$$

and

$$\Delta Y \leq 0.01\ cde^{-ay_o} \tag{25}$$

Since the number of grid increments in the X-direction must satisfy $M\Delta X = a$, while $N\Delta Y = c$,

$$M \geq \frac{10e^{bx_l}}{b}$$

and

$$N \geq \frac{50e^{dy_0}}{d} \tag{26}$$

The minimum number of grid points for acceptable resolution occurs when $b = 1/x_l$ and $d = 1/y_0$ and is given by

$$M \geq 10x_l e$$

and

$$N \geq 50y_o e \tag{27}$$

The boundary conditions in the transformed domain are:

$$\zeta(0, Y, t) = 0, \qquad \psi(0, Y, t) = 0, \tag{28}$$

$$\zeta(a, Y, t) = 0, \qquad \psi(a, Y, t) = 0, \tag{29}$$

$$\zeta(X, 0, t) = -c^2 d^2 \frac{\partial^2 \psi}{\partial Y^2}(X, 0, t), \tag{30}$$

$$\psi(X, 0, t) = 0, \tag{31}$$

$$\zeta(X, c, t) = 0, \quad \text{and} \quad \psi(X, c, t) = 0. \tag{32}$$

The discretized expression for the ground-plane vorticity, Eqn.(30), was developed by Roache (1972), and is given by

$$\zeta(X, 0, t) \approx -2\psi_n c^2 d^2 / \Delta Y^2 \tag{33}$$

where the subscript, n, indicates the grid locations adjacent to the ground plane.

In this study, the vertical grid spacing was fine enough to permit implementation of the no-slip boundary condition on the ground plane without exaggerating numerically the viscous interaction encountered previously by Delisi, Robins and Fraser (1987).

While the velocity boundary conditions appear to be over-specified (Anderson 1986), they are compatible with the velocity components in the transformed domain, given by

$$u = \frac{\partial \psi}{\partial Y} \cdot d \cdot (c - Y)$$
$$v = -\frac{\partial \psi}{\partial X} \cdot b \cdot (a - X) \qquad (34)$$

which can be easily verified. These boundary conditions also satisfy the integral conditions developed by Anderson (1986).

An alternating-direction implicit (ADI) scheme was used to solve the vorticity transport equation (1), with the upwind flux-splitting method applied to the convection terms and central-differencing for diffusion terms. An efficient Poisson solver (Swarztrauber and Sweet, 1979) was used to solve Eqn.(2). Viscous flow in a driven cavity was chosen as a test problem for that computational scheme to explore the capability of capturing the secondary-vortex evolution phenomena at high Reynolds number. The systematic numerical studies of this problem are well-documented in Bozeman and Dalton (1973) and Rubin and Harris (1975).

Stratification Effects

The present analysis has employed the Boussinesq approximations to model buoyancy effects. Specifically, the local density has been assumed related linearly to temperature via

$$\rho = \rho_0[1 - \alpha(T - T_0)] \qquad (35)$$

where α is the volumetric coefficient of thermal expansion and $\alpha \ll 1$. Hence, the density departure from the reference value can be represented in dimensionless form as

$$\tilde{\rho} = (\rho - \rho_0)/\rho_0 = -\alpha(T - T_0) \tag{36}$$

The complete Boussinesq model neglects all density variation effects except the body force term in the momentum equation so that the conservation of momentum equations result in the modified vorticity transport equation:

$$\frac{\partial \zeta}{\partial t} + \left(\vec{u} \cdot \vec{\nabla}\right)\zeta = -\frac{1}{F_v^2}\frac{\partial \tilde{\rho}}{\partial x} + \frac{1}{Re}\nabla^2\zeta \tag{37}$$

where

$$F_v^2 = \Gamma_0^2/g s_0^3 \tag{38}$$

For the case of a linearly stratified ambient fluid, the dimensionless temperature, θ, defined by

$$\theta \equiv (T - T_0)/T_0 \tag{39}$$

is assumed given in the quiescent, ambient state as

$$\bar{\theta} = \beta y \tag{40}$$

Hence, the ambient density departure is given by

$$\bar{\rho} = -\alpha\beta y T_0 \tag{41}$$

or

$$\bar{\theta} = -\bar{\rho}/\alpha T_0 \tag{42}$$

Similarly, the density and temperature fluctuations are related such that

$$\rho' = \tilde{\rho} - \bar{\rho}$$
$$\theta' = \theta - \bar{\theta} \tag{43}$$

and

$$\rho' = -\alpha T_0 \theta' \tag{44}$$

Neglecting viscous dissipation, the appropriate conservation of energy equation, invoking the Boussinesq approximation is:

$$\frac{\partial \theta}{\partial t} + \left(\vec{u} \cdot \vec{\nabla}\right)\theta = \frac{1}{R_e P_r}\nabla^2 \theta, \tag{45}$$

which can be written in terms of the density fluctuations (through Eqn. 44) for the stably stratified case as

$$\frac{\partial \rho'}{\partial t} + u\frac{\partial \rho'}{\partial x} + v\frac{\partial \rho'}{\partial y} + v\frac{d\bar{\rho}}{dy} = \frac{1}{RePr}\nabla^2 \rho' \tag{46}$$

Restricting attention to cases where $RePr \gg 1$, we can neglect the diffusion terms and the conservation of energy equation becomes:

$$\frac{\partial \rho'}{\partial t} + \left(\vec{u} \cdot \vec{\nabla}\right)\rho' = -v\frac{d\bar{\rho}}{dy}\,. \tag{47}$$

Alternatively, buoyancy effects could have been introduced through the compressible conservation of mass equation. By expanding the conservation of mass equation in terms of the volumetric coefficient of thermal expansion, α, the incompressible continuity equation and Eqn. (46) evolve from the zeroth and first order groupings in the α expansion. Hence, the numerical

simulation is modified via Eqns. (37), (41) and (47) when stratification effects are included. The computational scheme was easily modified to include stratification since the same grid was used and the density fluctuation equation could be implemented using the same procedures employed for the vorticity transport equation.

It is noted that the dimensionless parameter, F_v, which appears in the vorticity transport equation (37), is related to the Brunt-Väisälä frequency. That is, if the dimensionless density gradient is defined by

$$n^2 \equiv -\frac{d\bar{\rho}}{dy} \tag{48}$$

then the Brunt-Väisälä frequency, N, is given by

$$N^2 = -\frac{g}{s_0}\frac{d\bar{\rho}}{dy} = \frac{\Gamma_0^2 n^2}{s_0^4 F_v^2} \tag{49}$$

Stratification effects represent additional difficulties because of the characteristic time introduced via Brunt-Väisälä or density induced oscillations. If $s_0^2 N/\Gamma_0 (= \frac{n}{F_v}) \gg 1$, buoyancy effects are significant and the characteristic time (s_0^2/Γ_0) is large compared with the time interval over which density induced oscillations occur. The complication arising from these two characteristic times has been examined in detail by Hirsh (1985). For more realistic physical problems, F_v is typically quite large and the stratified density gradient (through n) is not large enough to result in large values of $s_0^2 N/\Gamma_0$. Consequently, a limiting test case is when the two time scales are equivalent $(s_0^2 N/\Gamma_0 \approx 1)$.

Simulations were run with $s_0^2 N/\Gamma_0 = 1$, but the density effects were so large that major vortices of opposite sign were generated very rapidly and the flow quickly became unstable numerically.

Ambient Turbulence

Inclusion of turbulent effects is an important element of this study. However, due to the approximate nature of turbulence models, initial work has restricted attention to limited types of turbulent processes and simple models. It is assumed here that atmospheric turbulence is being generated by axial (z-direction) wind shear. Since stratification effects are under investigation, it should be noted that buoyancy induced turbulence effects are usually small in the immediate vicinity of the ground, when compared to wind-driven fluctuations and have been neglected. However, some very important types of buoyancy-driven turbulence phenomena are known to occur with potentially serious consequences (e.g. microbursts), but those processes are too complicated to be modelled reliably at this time. These catastrophic-type, bouyancy-driven turbulence effects supercede wake-vortex prediction requirements and should be investigated separately. In addition, turbulence is generated by the wake vortex structures themselves. Those turbulence generation processes are also outside of the turbulence modelling capabilities employed in the present study.

The dimensionless vorticity transport equation can be written in index notation as

$$\frac{D\Omega_i}{Dt} - \Omega_j \frac{\partial u_i}{\partial x_j} = \frac{1}{R_e}\nabla^2\Omega_i \tag{50}$$

By assuming that the vorticity components can be decomposed into (slowly varying) time mean and (rapidly varying) unsteady parts, i.e.

$$\Omega_i = \bar{\Omega}_i + \Omega_i' \tag{51}$$

with

$$u_i = \bar{u}_i + u_i'$$

then the Reynolds averaged vorticity transport equation can be written:

$$\frac{\partial \bar{\Omega}_i}{\partial t} + \frac{\partial}{\partial x_j}(\bar{\Omega}_i \bar{u}_j) - \bar{\Omega}_j \frac{\partial \bar{u}_i}{\partial x_j} = \frac{1}{R_e}\nabla^2 \bar{\Omega}_i + \frac{\partial}{\partial x_j}\left(\overline{\Omega_j' u_i'}\right) - \frac{\partial}{\partial x_j}\left(\overline{u_j' \Omega_i'}\right) \tag{52}$$

Here, we restrict attention to mean flows which are steady and parallel in the z-direction, i.e. $\bar{w} = \bar{w}(y)$ so that

$$\bar{u} = \bar{u}(x, y, t) \tag{53}$$

and

$$\bar{v} = \bar{v}(x, y, t)$$

These are essentially two-dimensional flows, but permit the existence of two mean vorticity components. That is,

$$\bar{\Omega}_1 = \frac{d\bar{w}}{dy} = \bar{\Omega}_1(y)$$

and

$$\bar{\Omega}_3 = \bar{\zeta}(x, y, t), \tag{54}$$

with

$$\bar{\Omega}_2 = 0$$

Consequently, the governing equation on $\bar{\zeta}$ becomes:

$$\frac{\partial \bar{\zeta}}{\partial t} + \frac{\partial}{\partial x}(\bar{u}\bar{\zeta}) + \frac{\partial}{\partial y}(\bar{v}\bar{\zeta}) = \frac{1}{R_e}\nabla^2 \bar{\zeta} - \frac{\partial}{\partial x}\overline{u'\Omega_3'} - \frac{\partial}{\partial y}\left(\overline{v'\Omega_3'}\right) + \frac{\partial}{\partial x}\left(\overline{w'\Omega_1'}\right) + \frac{\partial}{\partial y}\left(\overline{w'\Omega_2'}\right) \tag{55}$$

where the $\overline{u_i'\Omega_j'}$ terms are the terms which must be modelled.

We have already stated that atmospheric turbulence has not been coupled with vortex-generated turbulence in this study. Essentially, it is assumed that the aircraft vorticity field behaves like a passive scalar, immersed in atmospheric turbulence. In that context, we have assumed that

$$\overline{\Omega_i' u_j'} = -c_1 q \Lambda \frac{\partial \bar{\Omega}_i}{\partial x_j} \tag{56}$$

where q^2 is the local turbulent kinetic energy,

$$q^2 = \frac{1}{2}\overline{u_k' u_k'} \ , \tag{57}$$

while Λ is a turbulent length scale and c_1 is the turbulence modelling constant. It is assumed that q and Λ are not altered by vortex interactions.

In order to utilize Eqn. (56), it is necessary to model q and Λ. Bilanin, Teske and Hirsh (1978) have employed a second order closure model, using similar nomenclature, to study vortex wake decay. When the wake vortex velocity field did not contribute to the turbulence, it was possible to show that q was constant both near the ground plane and in the far field. In addition, the von Karman constant, κ, can be used to model the characteristic turbulent length scale near the ground as

$$\Lambda \approx \kappa y \ . \tag{58}$$

Since Λ should be constant away from the ground, it was necessary to model the intermediate zone. Here, we have assumed that

$$\Lambda \approx c_2\left(1 - e^{-\kappa y / c_2}\right) \tag{59}$$

which matches Eqn. (58) for small y. von Karman's constant has been taken as 0.4 in this study, leaving c_2 as the remaining arbitrary constant.

Employing Eqn. (56) in Eqn. (55) yields:

$$\frac{\partial \bar{\zeta}}{\partial t} + \frac{\partial}{\partial x}(\bar{u}\bar{\zeta}) + \frac{\partial}{\partial y}(\bar{v}\bar{\zeta}) = \frac{1}{R_e}\nabla^2\bar{\zeta} + c_1 q \Lambda \frac{\partial^2 \bar{\zeta}}{\partial x^2} + c_1 q \frac{\partial}{\partial y}\left(\Lambda \frac{\partial \bar{\zeta}}{\partial y}\right) \tag{60}$$

where Λ is given by Eqns. (58) and (60) and c_1, c_2 and q are evaluated using experimental data.

Results

Based upon previous numerical studies, it was determined that the vortex core centers could be placed at $x_0 = 1$, $y_0 = 2$ (and $x_0 = -1$, $y_0 = 2$, from symmetry) to start the simulations. That vertical distance ($y_0 = 2$) was deemed close enough to the ground plane to produce detectable coupling effects after moderate time intervals after start-up, but it was also far enough from the ground plane to enable the vortex flow field to establish itself prior to strong ground-plane interactions. The initial vortex core was assumed to have a core radius, r_c, of 0.2 and a 150×300 grid was employed in the numerical simulations reported herein. Calculations were performed using a Cray II computer at NASA Langley Research Center.

Limited experimental data were available for numerical validation studies. Only the experiments of Liu and Srnsky (1990) were used. Their vortex flows were produced using an NACA 0012 wing model and the estimated circulation based Reynolds number (Γ_0/ν) was 7,650. Their experiments did not investigate stratification effects near a ground plane.

For the unstratified, validation studies, circulation Reynolds numbers of 1000, 7,650 and 75,000 were simulated. Figure 2(a) represents the trajectories ($x(t)$, $y(t)$) followed by the three simulated vortices, along with the measured trajectory of Liu and Srnsky (1990). The time histories of $x(t)$ and $y(t)$ for the four vortex cases are shown in Figures 2(b) and (c), respectively. The agreement between the numerical simulation and the experiment is quite good.

In order to assess the influence of Reynolds number, stratification and turbulence on the vortex hazard, some measure of hazard strength was required. However, since the computational domain is an unbounded quadrant, overall or global measures of circulation or velocity levels appeared to be of little value. It was finally decided that circulation and kinetic energy histories in the aircraft approach zone would be meaningful. The zone was selected somewhat arbitrarily to be the area bounded by $-2 < x < 2$ and $0 < y < 3$, which would span a typical runway entrance. The velocity components and vorticity were computed at each grid point within the right half of that area($0 < x < 2, 0 < y < 3$) at each time level. Subsequently, zonal circulation, $\Gamma(2\times3)$, was calculated by integrating the vorticity over the half area and the instantaneous kinetic energy within the zone, $E(2\times3)$, was computed by a similar integration of $\frac{(u^2+v^2)}{2}$. Those histories are shown in Figure 3 for the extreme Reynolds number cases(1000 and 75,000). The experiments of Liu and Srnsky did not report circulation and energy history data of this type.

Data were not available for comparison between simulated vortex flows in a stably stratified ambient environment with ground effect. Stratification effects were tested for a circulation-based Reynolds number of 1000, at dimensionless Brunt-Väisälä frequencies (n/F_v) of N = 0.05 and N = 0.1. The predicted results for this laminar flow case are displayed in Figure 4, along with the unstratified case (N = 0), for comparison. The trajectories, lateral and vertical position histories, along with circulation strength $\Gamma(2\times3)$ and kinetic energy $E(2\times3)$ histories are displayed in Figures 4(a) through (e), respectively.

The background turbulence model, discussed in the previous section, was incorporated in the simulations for a circulation-based Reynolds number of 75,000. A global turbulence constant, C, defined by

$$C \equiv c_1 c_2 q$$

is all that is required to model this eddy-viscosity type turbulence (since c_2 was chosen as 0.5) and values of C = 0.001 and 0.1 were employed in the simulations. The combined effects of Reynolds number, turbulence and ground effect on vortex motion and strength are shown in Figures 5.

Discussion

While the laminar flow simulations (Re = 1000) are less realistic, in terms of aircraft vortices, they are less ambiguous, in terms of effects of turbulence models and numerical uncertainties. Consequently, vortex rebound and stratification effects, derived from fundamental phenomena, can be discussed with more certainty for those flow cases. To that end, stratification effects in the vicinity of the ground plane have altered vortex trajectories rather remarkably, as shown in Figure 4.

Referring to Figure 4, it can be seen that the vortex appears to literally try to "fall back down hill" in both stratified cases, even though the initial descent and rebound trajectories nearly coincide with the unstratified case. The mechanism which is responsible for that effect can best be explained by comparing the computational flow visualization results from the unstratified case (N = 0) with the stratified case (N = 0.1).

Figures 6 and 7 are color panels comparing the vorticity distributions at four time levels for an unstratified flow (Figure 6) and a stratified flow (Figure 7). Streamfunction contours are compared in Figures 8 and 9.

The stratification effect on vortex trajectory is most easily understood by looking at the density distribution. Figure 10, shows density departure contours (from Eqn. 41, via ρ', given in Eqn. 43) at four different times. There, it can be seen that relatively higher density fluid is pulled from the ground plane around the primary vortex, where it tends simultaneously to compress the vortex and cause more rapid vortex deceleration due to increased inertia. While

the vortex doesn't actually roll back toward the ground by reversing itself like a wheel, the density distributions show that the body forces actually push the primary vortex back toward the ground plane and the lateral density variations even push the vortex toward the symmetry plane. Clearly, density stratification can confine then destroy trailing line vortices much more rapidly than any other process considered in this study.

Conclusions

This study has shown that trailing line vortex flows can be resolved in the vicinity of a ground plane. Vortex trajectory comparisons with the experimental measurements of Liu and Srnsky are in quite good agreement. The preliminary inclusion of modelled turbulence effects has not produced any startling results. On the other hand, density stratification can have a very pronounced effect on vortex trajectories. At the admittedly high stratification levels considered here, we have shown that vortex hazard alleviation could be facilitated by density stratification effects within the immediate vicinity of airport runways.

Acknowledgment

This work was sponsored by NASA Langley Research Center under Research Grants NAG1-987 and NAG1–530. The authors would like to thank Mr. George C. Greene for his helpful suggestions and stimulating discussions.

References

Anderson, C. R. 1986 On vorticity boundary conditions. Center for Large Scale Scientific Computation, Stanford University, Report CLaSSiC 86–14.

Ash, R. L. and Zheng, Z. 1991. NASA Contractor Report.

Baker, S. J. and Crow, S. C. 1977 The motion of two-dimensional vortex pairs in ground effect. *J. Fluid Mech.* **82**, 659–671.

Bilanin, A. J., Teske, M. E., Donaldson, C. duP. and Williamson, G. G. 1977 Vortex interactions and decay in aircraft wakes. NASA Contractor Report, NASA CR-2870.

Bilanin, A. J., Teske, M. E. and Hirsh, J. E. 1978 Neutral atmospheric effects on the dissipation of aircraft vortex wakes. *AIAA J.* **16**, 956–961.

Bozeman, J. D. and Dalton, C. 1973 Numerical study of viscous flow in a cavity. *J. Computational Physics* **12**, 348–363.

Delisi, D. P., Robins, R. E. and Fraser, R. B. 1987 The effects of stratification and wind shear on the evolution of aircraft wake vortices near the ground: Phase I Results. Northwest Research Associates, Inc. NWRA-87-R006.

Greene, G. C. 1986 An approximate model of vortex decay in the atmosphere. *J. Aircraft* **23**, 566–573.

Harvey, J. K. and Perry, F. J. 1971 Flowfield produced by trailing vortices in the vicinity of the ground. *AIAA J.* **9**, 1659–1660.

Hirsh, R. S. 1985 A numerical simulation of vortex motion in a stratified environment and comparison with experiments. Johns Hopkins APL Technical Digest, **6**, 203–210.

Liu, C. H. and Ting, L. 1987 Interaction of decaying trailing vortices in spanwise shear flow. *Computers & Fluids* **15**, 77–92.

Liu, H. T. and Srnsky R. A. 1990 Laboratory investigation of atmospheric effects on vortex wakes. Flow Research Inc. Technical Report No. 497.

Oseen, C. W. 1911 Über wirbelbewegung in einer meibenden flüssigkeit. Arkiv För Matematic, Astronomi Och Fysik 7, 1–13.

Peace, A. J. and Riley, N. 1983 A viscous vortex pair in ground effect. *J. Fluid Mech.* **129**, 409–426.

Roach, P. J. 1972 *Computational Fluid Dynamics*, Hermosa Pub.

Rubin, S. G. and Harris, J. E. 1975 Numerical studies of incompressible viscous flow in a driven cavity. NASA SP-378.

Saffman, P. G. 1979 The approach of a vortex pair to a plane surface in inviscid fluid. *J. Fluid Mech.* **92**, 497–503.

Swarztrauber, P. N. and Sweet, R. A. 1979 Algorithm 541, Efficient FORTRAN subprograms for the solution of separable elliptic partial differential equations [D3]. ACM Trans. on Math. Software **5**, 352–364.

Ting, L. 1983 On the application of the integral invariants and decay laws of vorticity distributions. *J. Fluid Mech.* **127**, 497–506.

Appendix A. Asymptotic Solution for Flow Field Initialization

Asymptotic expansions, in terms of $\epsilon = \sqrt{t/R_e}$, were used in both the outer flow and the inner flow. The two-dimensional, unsteady incompressible, Navier-Stokes equations were used as the governing equations in both regions. Employing van Dyke (1976) type matching procedures, the streamfunction and velocity, as well as pressure, were matched asymptotically. Analytic solutions were obtained when the inner solution was expanded further in time.

In the following development, a two-term expansion is represented for this application. First, the expansion for streamfunction and velocity are presented. Then matching conditions are obtained by switching outer and inner variables according to van Dyke's (1976) procedure. Since pressure can be derived if the velocity field is known in an incompressible flow, pressure matching is accomplished through the governing equations and will be developed after the governing equations in both regions are discussed. Finally, a closed form solution for the two-term expansions is developed.

Expansions and Matching for Streamfunction and Velocity

The appropriate streamfunction for the outer flow can be written

$$\Psi = \Psi_o(x, y, t) + \epsilon\Psi_1(x, y, t) + O\left[\epsilon^2\right], \tag{A.1}$$

where

$$U = \frac{\partial\Psi}{\partial y} = \frac{\partial\Psi_o}{\partial y} + \epsilon\frac{\partial\Psi_1}{\partial y} + O\left[\epsilon^2\right] \tag{A.2}$$

and

$$V = -\frac{\partial\Psi}{\partial x} = -\frac{\partial\Psi_o}{\partial x} - \epsilon\frac{\partial\Psi_1}{\partial x} + O\left[\epsilon^2\right] \tag{A.3}$$

Similarly, the inner flow is represented as

$$\psi = 2\epsilon[\psi_o(x, \eta, t) + \epsilon\psi_1(x, \eta, t)] + O\left[\epsilon^3\right] \tag{A.4}$$

where

$$\eta = y/2\epsilon.$$

Here, the inner velocity components are

$$\begin{aligned} u = \frac{\partial \psi}{\partial y} &= 2\epsilon\left(\frac{1}{2\epsilon}\frac{\partial \psi_o}{\partial \eta} + \frac{1}{2}\frac{\partial \psi_1}{\partial \eta}\right) + O\left[\epsilon^2\right] \\ &= \frac{\partial \psi_o}{\partial \eta} + \epsilon\frac{\partial \psi_1}{\partial \eta} + O\left[\epsilon^2\right] \end{aligned} \tag{A.5}$$

and

$$v = -\frac{\partial \psi}{\partial x} = -2\epsilon\left(\frac{\partial \psi_o}{\partial x} + \epsilon\frac{\partial \psi_1}{\partial x}\right) + O\left[\epsilon^3\right] \tag{A.6}$$

Matching Conditions

Following van Dyke's (1976) matching theorem, we rewrite the outer expansion in inner variable η, while the inner expansion is rewritten in outer variable y. We then rewrite both the streamfunction and the velocity and match the corresponding terms. It is shown subsequently that using this matching procedure allows the streamfunction and velocity to be matched simultaneously.

Rewriting the outer expansion in inner variables and expanding in terms of ϵ, we have

$$\begin{aligned} \Psi &= \Psi_o(x, 2\epsilon\eta, t) + \epsilon\Psi_1(x, 2\epsilon\eta, t) + O\left[\epsilon^2\right] \\ &\approx \Psi_o(x, 0, t) + \epsilon\left[2\eta\frac{\partial \Psi_o}{\partial y}(x, 0, t) + \Psi_1(x, 0, t)\right] + O\left[\epsilon^2\right] \end{aligned} \tag{A.7}$$

$$U \approx \frac{\partial \Psi_o}{\partial y}(x, 0, t) + \epsilon\left[2\eta\frac{\partial^2 \Psi_o}{\partial y^2}(x, 0, t) + \frac{\partial \Psi_1}{\partial y}(x, 0, t)\right] + O\left[\epsilon^2\right] \tag{A.8}$$

$$V \approx -\frac{\partial \Psi_o}{\partial x}(x, 0, t) - \epsilon\left[2\eta\frac{\partial^2 \Psi_o}{\partial x \partial y}(x, 0, t) + \frac{\partial \Psi_1}{\partial x}(x, 0, t)\right] + O\left[\epsilon^2\right] \tag{A.9}$$

Rewriting the inner expansion in outer variables and expanding in terms of ϵ,

$$\begin{aligned}\psi &= 2\epsilon\left[\psi_o\left(x, \frac{y}{2\epsilon}, t\right) + \epsilon\psi_1\left(x, \frac{y}{2\epsilon}, t\right)\right] + O\left[\epsilon^3\right] \\ &\approx 2\epsilon\psi_o(x, \infty, t) + O\left[\epsilon^2\right]\end{aligned} \tag{A.10}$$

$$u \approx \frac{\partial\psi_o}{\partial\eta}(x, \infty, t) + \epsilon\frac{\partial\psi_1}{\partial\eta}(x, \infty, t) + O\left[\epsilon^2\right] \tag{A.11}$$

$$v \approx -2\epsilon\frac{\partial\psi_o}{\partial x}(x, \infty, t) + O\left[\epsilon^2\right] \tag{A.12}$$

From Eqns. (A.10), (A.11) and (A.12), one can see that in the boundary layer the streamfunction and y-component of velocity is one order lower in ϵ than the x-component of velocity.

Now we match streamfunction, x-component of velocity and y-component velocity, respectively, but to different order. We obtain

$O[\epsilon^o]$:

$$\Psi_o(x, 0, t) = 0 \tag{A.13}$$

$$\frac{\partial\Psi_o}{\partial y}(x, 0, t) = \frac{\partial\psi_o}{\partial\eta}(x, \infty, t) = U_o \tag{A.14}$$

$$\frac{\partial\Psi_o}{\partial x}(x, 0, t) = 0 \tag{A.15}$$

$O[\epsilon^1]$:

$$\left[2\eta\frac{\partial\Psi_o}{\partial y}(x, 0, t) + \Psi_1(x, 0, t)\right]_{\eta\to\infty} = 2\psi_o(x, \eta, t)\Big|_{\eta\to\infty} \tag{A.16}$$

$$\left[2\eta\frac{\partial^2\Psi_o}{\partial y^2}(x, 0, t) + \frac{\partial\Psi_1}{\partial y}(x, 0, t)\right]_{\eta\to\infty} = \frac{\partial\psi_1}{\partial\eta}(x, \eta, t)\Big|_{\eta\to\infty} \tag{A.17}$$

$$\left[-2\eta\frac{\partial^2\Psi_o}{\partial x\partial y}(x,0,t)-\frac{\partial\Psi_1}{\partial x}(x,0,t)\right]_{\eta\to\infty}=-2\frac{\partial\psi_o}{\partial x}(x,\eta,t)\Big|_{\eta\to\infty} \tag{A.18}$$

As expected, Eqns. (A.13)-(A.18) either give the bottom boundary condition for the outer flow or the top boundary condition of the inner-flow. Equations (A.13) and (A.15) are equivalent and they just give one boundary condition for Ψ_o which is obviously the slip-free boundary condition. Equation (A.14) is the top boundary condition for ψ_o which must match (at the edge) the x-component of velocity, U_o. Equations (A.16) and (A.18) are also equivalent and they provide a boundary condition for Ψ_1, while Eqn. (A.17) is a boundary condition for ψ_1. The equivalence between Eqns. (A.13) and (A.15), (A.16) and (A.18) shows that the streamfunction and velocity matching can be achieved simultaneously without contradiction in this procedure. The physical boundary conditions are thus retained by the mathematical manipulation.

From the matching procedure, the solution for the two series can proceed sequentially; first the outer solution Ψ_o, then the inner solution ψ_o can be developed; followed by solution of Ψ_1, and so on.

Governing Equations

As stated previously, the governing equations used are the two-dimensional unsteady, incompressible Navier-Stokes equations. Since continuity is implied by introducing the streamfunction, we will concentrate on the momentum equations.

Outer Flow

Because viscous terms do not have any direct effect until terms of order ϵ^2 are important, it is not necessary to include viscous effects for the two-term outer solution. Thus, we have

$$\frac{\partial U}{\partial t}+U\frac{\partial U}{\partial x}+V\frac{\partial U}{\partial y}=-\frac{\partial P}{\partial x} \tag{A.19}$$

$$\frac{\partial V}{\partial t} + U\frac{\partial V}{\partial x} + V\frac{\partial V}{\partial y} = -\frac{\partial P}{\partial y} \tag{A.20}$$

In addition, if we assume the flow is irrotational — especially near the edge of the boundary layer — the potential flow relation

$$\nabla^2 \Psi = 0 \tag{A.21}$$

can be used instead of Eqns. (A.19) and (A.20). That has been done here and the Euler equations have been used only to determine the pressure field.

For different orders of ϵ, we get

$$O[\epsilon^o]: \quad \nabla^2 \Psi_o = 0 \tag{A.22}$$

$$O[\epsilon^1]: \quad \nabla^2 \Psi_1 = 0 \tag{A.23}$$

Since the outer solution here is only used for the purpose of generating the boundary-layer solution, the potential solution may or may not be applied to the whole outer flow field.

Inner Flow

The dimensionless component of the boundary layer momentum equation can be written

$$\frac{\partial u}{\partial t} + u\frac{\partial u}{\partial x} + v\frac{\partial u}{\partial y} = -\frac{dp}{dx} + \frac{1}{Re}\frac{\partial^2 u}{\partial y^2} \tag{A.24}$$

when we have already assumed $\frac{\partial^2 u}{\partial x^2}$ and $\frac{\partial P}{\partial y}$ can be neglected because both terms do not appear in the first two terms of the solution. From Eqns. (A.4) and (A.5), we get

$$\frac{\partial u}{\partial t} = \frac{\partial^2 \psi_o}{\partial \eta \partial t} - \frac{\eta}{2t}\frac{\partial^2 \psi_o}{\partial \eta^2} + \epsilon\left[\frac{1}{2t}\frac{\partial \psi_1}{\partial \eta} + \frac{\partial^2 \psi_1}{\partial \eta \partial t} - \frac{\eta}{2t}\frac{\partial^2 \psi_1}{\partial \eta^2}\right] + O[\epsilon^2] \tag{A.25}$$

$$\frac{\partial u}{\partial y} = \frac{1}{2\epsilon}\left[\frac{\partial^2 \psi_o}{\partial \eta^2} + \epsilon \frac{\partial^2 \psi_1}{\partial \eta^2}\right] + O[\epsilon] \tag{A.26}$$

and

$$\frac{\partial^2 u}{\partial y^2} = \frac{1}{4\epsilon^2}\left[\frac{\partial^3 \psi_o}{\partial \eta^3} + \epsilon \frac{\partial^3 \psi_1}{\partial \eta^3}\right] + O[\epsilon^o] \tag{A.27}$$

If we let

$$p = p_o(x,t) + \epsilon p_1(x,t) + O\left[\epsilon^2\right], \tag{A.28}$$

these expressions (Eqns. A.25–A.28) along with Eqn. (A.6) can be substituted into Eqn. (A.24), to obtain the equations for different orders of ϵ:

$O[\epsilon^o]$:

$$\begin{aligned} &\frac{\partial^2 \psi_o}{\partial \eta \partial t} - \frac{\eta}{2t}\frac{\partial^2 \psi_o}{\partial \eta^2} + \frac{\partial \psi_o}{\partial \eta}\frac{\partial^2 \psi_o}{\partial \eta \partial x} - \frac{\partial^2 \psi_o}{\partial \eta^2}\frac{\partial \psi_o}{\partial x} \\ &\qquad = -\frac{dp_o}{dx} + \frac{1}{4t}\frac{\partial^3 \psi_o}{\partial \eta^3} \end{aligned} \tag{A.29}$$

The three boundary conditions are the non-slip boundary condition and matching conditions: (from Eqn. A.14):

$$\psi_o(x,0,t) = 0 \tag{A.30}$$

$$\frac{\partial \psi_o}{\partial \eta}(x,0,t) = 0 \tag{A.31}$$

$$\frac{\partial \psi_o}{\partial \eta}(x,\infty,t) = \frac{\partial \Psi_o}{\partial y}(x,0,t) = U_o \tag{A.32}$$

$O\left[\epsilon^1\right]$:

$$\begin{aligned} &\frac{1}{2t}\frac{\partial \psi_1}{\partial \eta} + \frac{\partial^2 \psi_1}{\partial \eta \partial t} - \frac{\eta}{2t}\frac{\partial^2 \psi_1}{\partial \eta^2} + \frac{\partial \psi_o}{\partial \eta}\frac{\partial^2 \psi_1}{\partial \eta \partial x} \\ &\qquad + \frac{\partial \psi_1}{\partial \eta}\frac{\partial^2 \psi_o}{\partial \eta \partial x} - \frac{\partial \psi_o}{\partial x}\frac{\partial^2 \psi_1}{\partial \eta^2} - \frac{\partial \psi_1}{\partial x}\frac{\partial^2 \psi_o}{\partial \eta^2} \\ &\qquad = -\frac{dp_1}{dx} + \frac{1}{4t}\frac{\partial^3 \psi_1}{\partial \eta^3} \end{aligned} \tag{A.33}$$

The three boundary conditions for ψ_1 are no-slip conditions and matching condition Eqn. (A.17):

$$\psi_1(x,0,t) = 0 \tag{A.34}$$

$$\frac{\partial \psi_1}{\partial \eta}(x,0,t) = 0 \tag{A.35}$$

$$\frac{\partial \psi_1}{\partial \eta}(x,\eta,t)\Big|_{\eta\to\infty} = \left[2\eta \frac{\partial^2 \Psi_o}{\partial y^2}(x,0,t) + \frac{\partial \Psi_1}{\partial y}(x,0,t)\right]_{\eta\to\infty} \tag{A.36}$$

From Eqn. (A.22), we have

$$\frac{\partial^2 \Psi_o}{\partial x^2}(x,0,t) + \frac{\partial^2 \Psi_o}{\partial y^2}(x,0,t) = 0$$

while Eqn. (A.13) yields $\Psi_o(x,0,t) = 0$.

Hence

$$\frac{\partial^2 \Psi_o}{\partial y^2}(x,0,t) = -\frac{\partial^2 \Psi_o}{\partial x^2}(x,0,t) = \frac{\partial^2 \Psi_o(x,0,t)}{\partial x^2} = 0 \tag{A.37}$$

Therefore, Eqn. (A.36) can be rewritten:

$$\frac{\partial \psi_1}{\partial \eta}(x,\infty,t) = \frac{\partial \Psi_1}{\partial y}(x,0,t) = U_1 \tag{A.38}$$

Pressure Gradient Matching

As mentioned earlier, to second order we have $\frac{\partial P}{\partial y} = 0$ in the boundary layer for the asymptotic expansions developed here. Consequently, we have

$$\frac{\partial P}{\partial x}\Big|_{y=0} = \frac{dp}{dx} \tag{A.39}$$

From the governing equation for the outer flow (Eqn. A.19), we have

$$\left.\frac{\partial U}{\partial t}\right|_{y=0} + U\left.\frac{\partial U}{\partial x}\right|_{y=0} = \left.\frac{\partial P}{\partial x}\right|_{y=0} \tag{A.40}$$

Since from Eqn. (A.2)

$$\frac{\partial U}{\partial t} = \frac{\partial^2 \Psi_o}{\partial y \partial t} + \epsilon \frac{\partial^2 \Psi_1}{\partial y \partial t} + \frac{1}{2t}\epsilon \frac{\partial \Psi}{\partial y} \quad , \tag{A.41}$$

we obtain

$O[\epsilon^o]$:

$$\frac{\partial U_o}{\partial t} + U_o \frac{\partial U_o}{\partial x} = -\frac{dp_o}{dx} \tag{A.42}$$

$O[\epsilon^1]$:

$$\frac{\partial U_1}{\partial t} + \frac{1}{2t}U_1 + U_o \frac{\partial U_1}{\partial x} + U_1 \frac{\partial U_o}{\partial x} = -\frac{dp_1}{dx} \tag{A.43}$$

Solution for Inner Flow

From Nam (1990), it is known that in an unsteady boundary layer, a two-series expansion is needed, in terms of ϵ and t. In the following, we write each inner solution in different orders of ϵ as a power series in terms of t. Since we just use the solution as the initial condition in this problem, we can choose small t and then only the first several terms are needed. A closed form solution is thus obtained for the first two terms of the expansions.

$O[\epsilon^o]$:

Let

$$\psi_o = \sum_{p=0}^{\infty} t^p \phi_p^o(x, \eta, t) \tag{A.44}$$

Then the first two terms are:

$$\psi_o = U_o f_{01} + t\left(\frac{\partial U_o}{\partial t} f_{11} + U_o \frac{\partial U_o}{\partial x} f_{12}\right) + O\left[t^2\right] \tag{A.45}$$

Substituting Eqn. (A.45) into Eqn. (A.29), with boundary conditions, Eqns. (A.30), (A.31), (A.32) and employing the pressure gradient Eqn. (A.42), we obtain, for different orders of t:

$O[t^o]$:

$$f_{o1}''' + 2\eta f_{01}'' = 0, \tag{A.46}$$

subject to:

$$f_{01}(0) = f_{01}'(0) = 0 \tag{A.47}$$

$$f_{01}'(\infty) = 1 \tag{A.48}$$

$O\left[t^1\right]$:

$$f_{11}''' + 2\eta f_{11}'' - 4f_{11}' = -4 + 4f_{01}' \tag{A.49}$$

subject to:

$$f_{11}(0) = f_{11}'(0) = 0 \tag{A.50}$$

$$f_{11}'(\infty) = 0 \tag{A.51}$$

and

$$f_{12}''' + 2\eta f_{12}'' - 4f_{12}' = -4 + 4\left(f_{01}'\right)^2 - 4f_{01}f_{01}' \tag{A.52}$$

subject to:

$$f_{12}(0) = f_{12}'(0) = 0 \tag{A.53}$$

$$f'_{12}(\infty) = 0 \tag{A.54}$$

The solutions for f_{01}, f_{11} and f_{12} are given in the text as Eqns. (11)-(13).

$O[\epsilon^1]$:

Let

$$\psi_1 = \sum_{p=0}^{\infty} t^p \phi_p^1(x, \eta, t) \tag{A.55}$$

Then the first two terms

$$\psi_1 = U_1 g_{01} + t\left(\frac{\partial U_1}{\partial t} g_{11} + U_o \frac{\partial U_1}{\partial x} g_{12} + U_1 \frac{\partial U_o}{\partial x} g_{13}\right) + O[t^2] \tag{A.56}$$

are gotten by substituting Eqn. (A.56) into Eqn. (A.33), with boundary conditions Eqns. (A.34), (A.35) and (A.36) and pressure gradient condition Eqn. (A.43). We obtain for different orders of t

$O[t^o]$:

$$g'''_{01} + 2\eta g''_{01} - 2g'_{01} = -2 \tag{A.57}$$

subject to

$$g_{01}(0) = g'_{01}(0) = 0 \tag{A.58}$$

$$g'_{01}(\infty) = 1 \tag{A.59}$$

$O[t^1]$:

$$g'''_{11} + 2\eta\, g''_{11} - 6g'_{11} = -4 + 4g'_{01} \tag{A.60}$$

subject to:

$$g_{11}(0) = g'_{11}(0) = 0 \tag{A.61}$$

$$g'_{11}(\infty) = 0 \tag{A.62}$$

and

$$g'''_{12} + 2\eta g''_{12} - 6g'_{12} = -4 + 4f'_{01}g'_{01} \tag{A.63}$$

subject to:

$$g_{12}(0) = g'_{12}(0) = 0 \tag{A.64}$$

$$g'_{12}(\infty) = 0 \tag{A.65}$$

and

$$g'''_{13} + 2\eta\, g'_{13} - 6g_{13} = -4 + 4f'_{01}g'_{01} - 4f_{01}g''_{01}$$

subject to:

$$g_{13}(0) = g'_{13}(0) = 0 \tag{A.66}$$

$$g'_{13}(\infty) = 0 \tag{A.67}$$

The solutions for g_{01}, g_{11}, g_{12} and g_{13} are given in the text as Eqns. (14)-(17).

Appendix B. Derivation of Fluctuation Density Equation through Conservation of Mass

In incompressible flow, the local density is a function of temperature and here it is assumed linearly related to temperature via

$$\rho = \rho_o[1 - \alpha(T - T_o)] \tag{B.1}$$

where α is the volumetric coefficient of thermal expansion and $\alpha << 1$.

We define dimensionless density and temperature as

$$\tilde{\rho} \equiv (\rho - \rho_o)/\rho_o \tag{B.2}$$

$$\theta = (T - T_o)/T_o \tag{B.3}$$

respectively.

For the case of a linearly stratified ambient fluid, the quiescent ambient state, $\bar{\theta}$, is assumed given by

$$\bar{\theta} = \beta y \tag{B.4}$$

Hence, the ambient density departure is

$$\bar{\rho} = -\alpha(\bar{T} - T_o) = -\alpha\beta y T_o \tag{B.5}$$

and

$$\frac{d\bar{\rho}}{dy} = -\alpha\beta T_o \tag{B.6}$$

Now, with the density fluctuation and temperature fluctuation defined as

$$\rho' \equiv \tilde{\rho} - \bar{\rho} \tag{B.7}$$

$$\theta' \equiv \theta - \bar{\theta} \tag{B.8}$$

we have

$$\rho' = -\alpha T_o \theta' \tag{B.9}$$

From the continuity equation for compressible flow

$$\frac{\partial \rho}{\partial t} + u\frac{\partial \rho}{\partial x} + v\frac{\partial \rho}{\partial y} + \rho\vec{\nabla}\cdot\vec{u} = 0, \tag{B.10}$$

we obtain the dimensionless equation

$$\frac{\partial \tilde{\rho}}{\partial t} + u\frac{\partial \tilde{\rho}}{\partial x} + v\frac{\partial \tilde{\rho}}{\partial y} + (1+\tilde{\rho})\vec{\nabla}\cdot\vec{u} = 0 \tag{B.11}$$

Substituting Eqn. (B.7) into Eqn. (B.11), we get

$$\frac{\partial \rho'}{\partial t} + u\frac{\partial \rho'}{\partial x} + v\frac{\partial \rho'}{\partial y} + v\frac{d\bar{\rho}}{dy} + \vec{\nabla}\cdot\vec{u} + (\bar{\rho}+\rho')\vec{\nabla}\cdot\vec{u} = 0 \tag{B.12}$$

From Eqns. (B.6) and (B.9), one can see that

$$\frac{d\bar{\rho}}{dy} \sim O[\alpha]$$

$$\rho' \sim O[\alpha]$$

Hence, for terms of $O[\alpha^o]$, Eqn. (B.12) gives

$$\vec{\nabla}\cdot\vec{u} = 0 \tag{B.13}$$

which recovers incompressibility.

Then for $O[\alpha]$, Eqn. (B.12) gives

$$\frac{\partial \rho'}{\partial t} + u\frac{\partial \rho'}{\partial x} + v\frac{\partial \rho'}{\partial y} = -v\frac{d\bar{\rho}}{dy} \tag{B.14}$$

which is the same as Eqn. (47) in the text, which was derived from the conservation of energy equation.

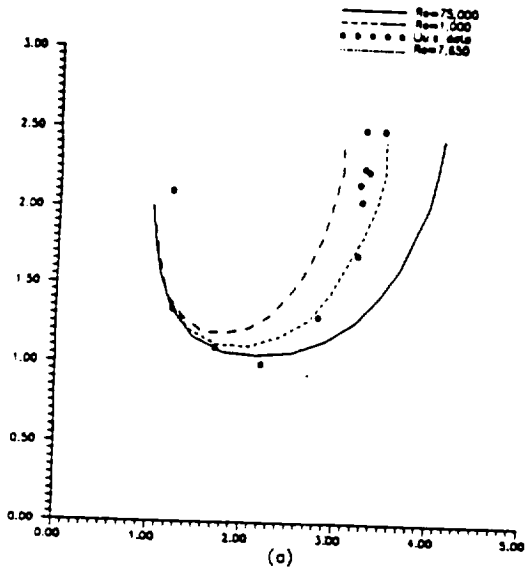

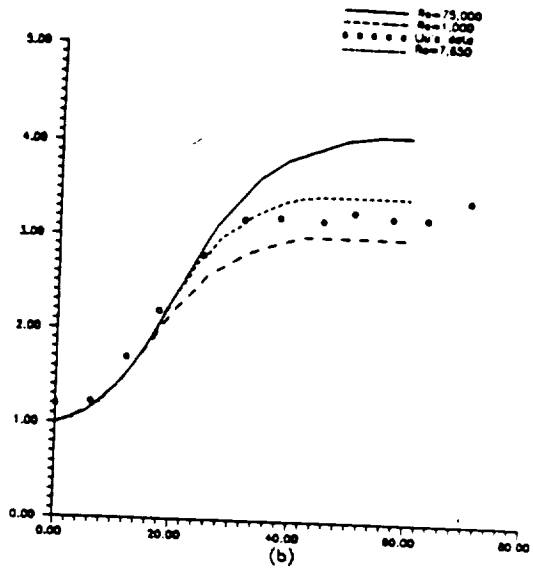

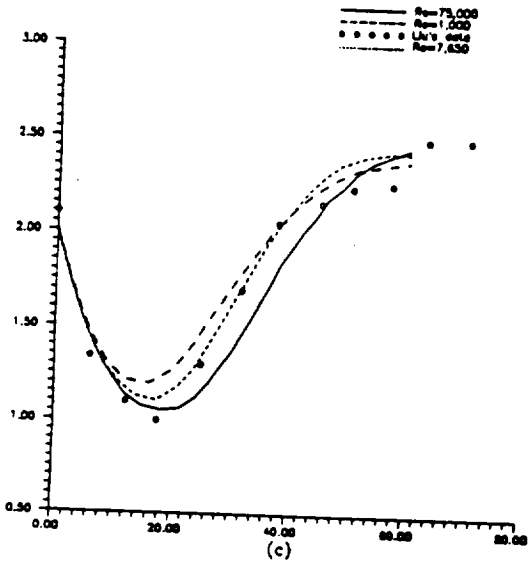

Figure 2. Comparison between computed and meassured (a) vortex trajectories, (b) lateral vortex position histories, (c) vortex elevation histories, at various Reynolds numbers

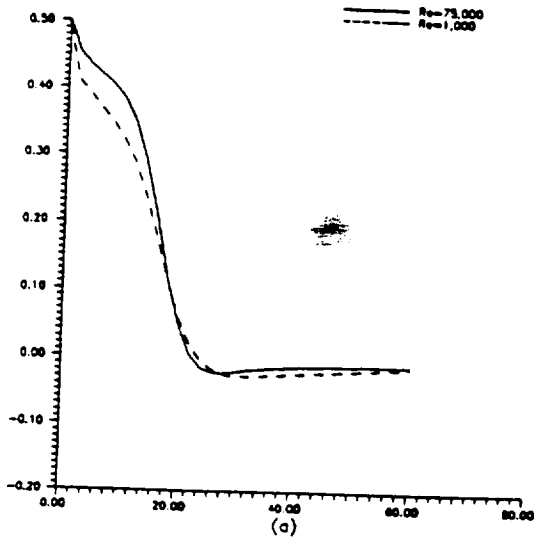

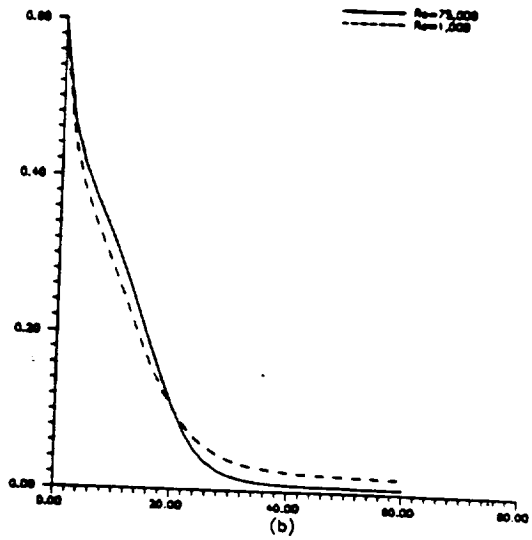

Figure 3. Predicted variation of (a) circulation $\Gamma(2\times3)$, (b) kinetic energy $E(2\times3)$, with time for various Reynolds numbers

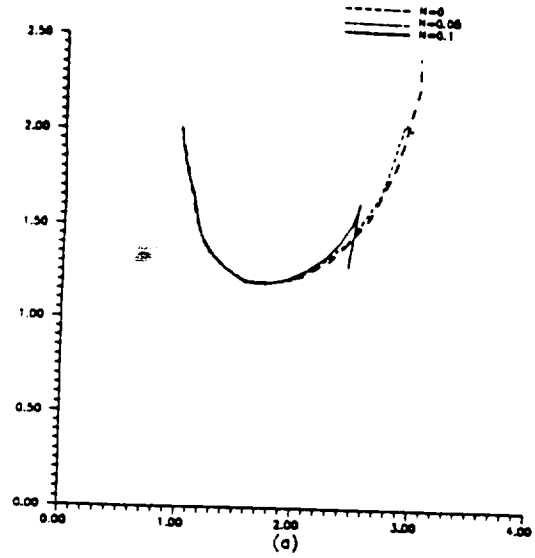

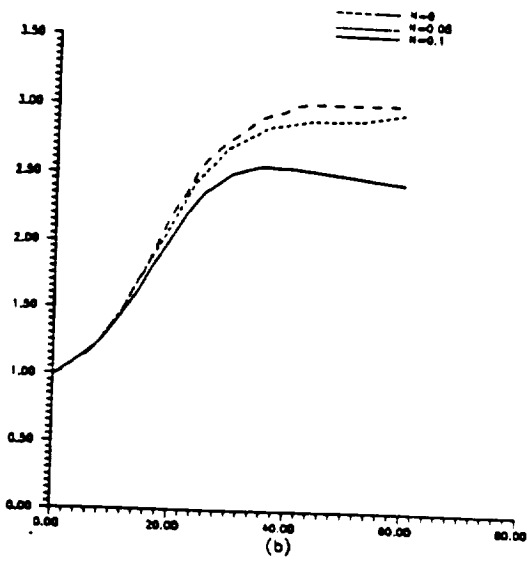

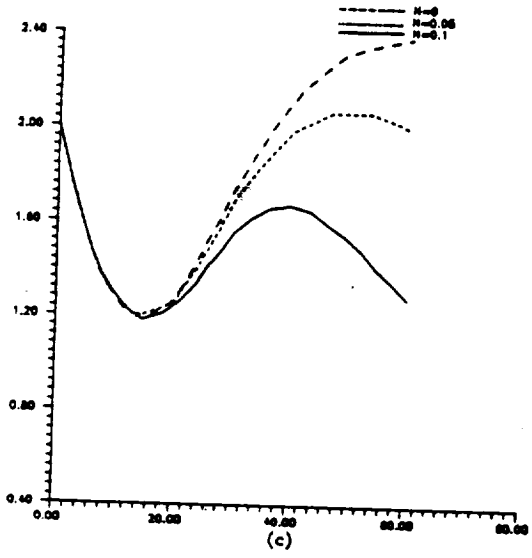

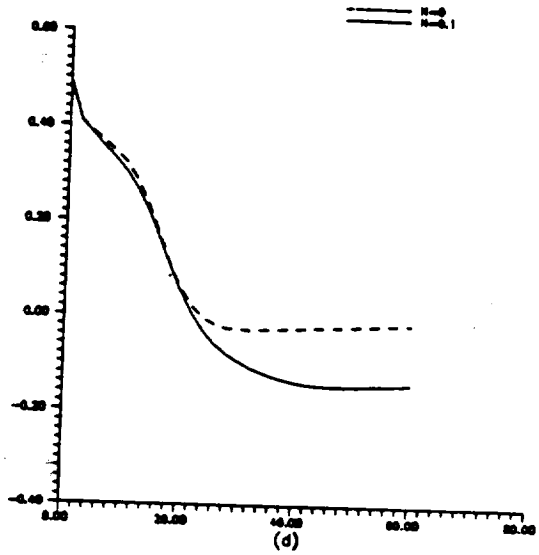

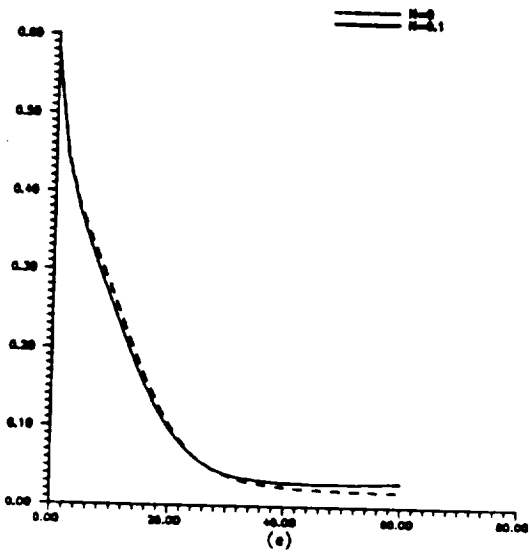

Figure 4. Influence of stratification on predicted (a) vortex trajectories, (b) lateral vortex position histories, (c) elevation histories, (d) circulation $\Gamma(2\times3)$, (e) kinetic energy $E(2\times3)$, Re=1,000

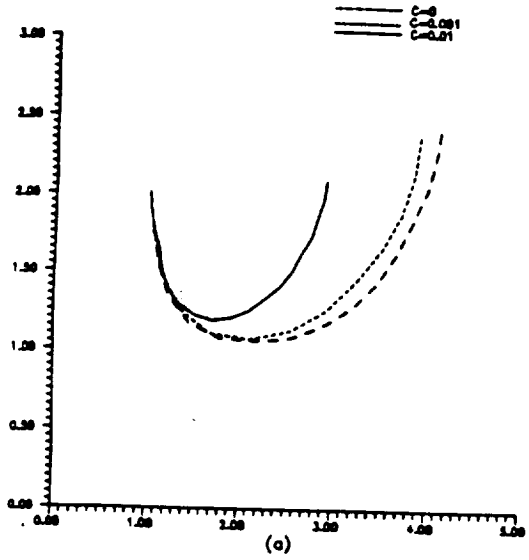

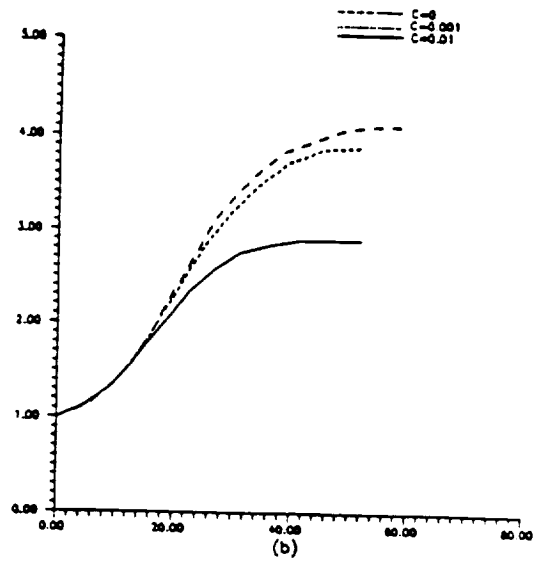

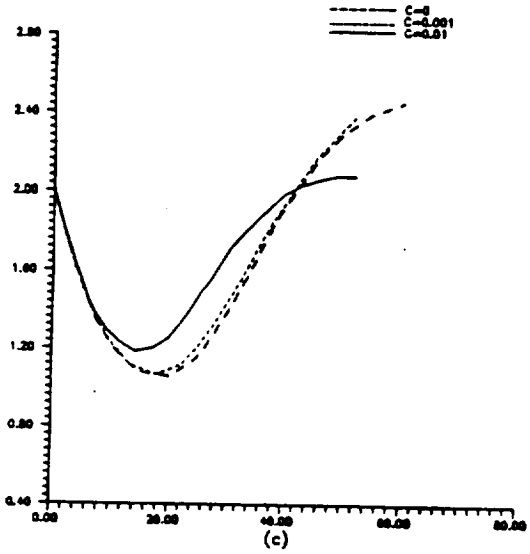

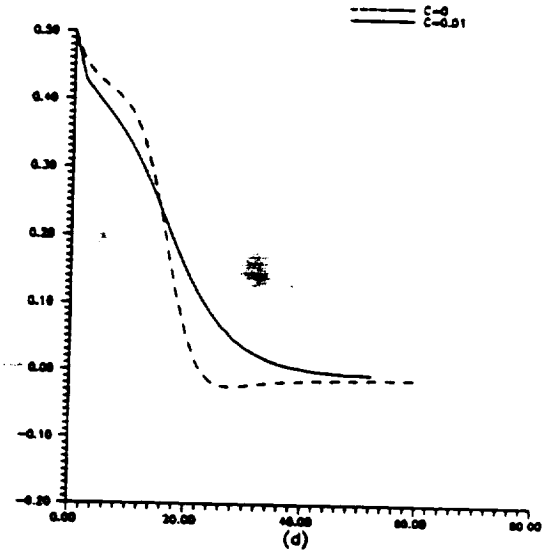

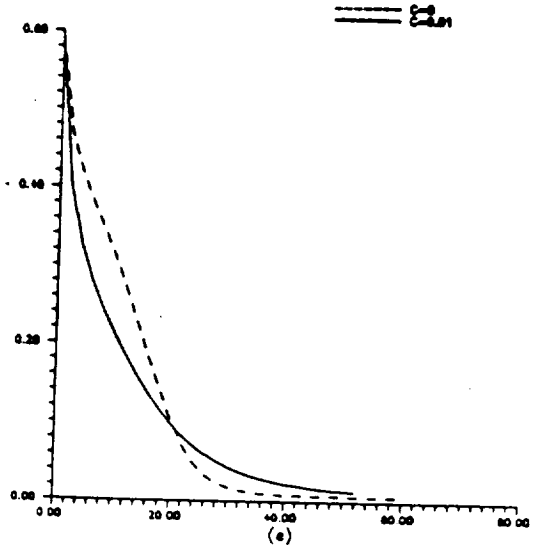

Figure 5. Influence of turbulence on predicted (a) vortex trajectories, (b) lateral vortex position histories, (c) elevation histories, (d) circulation $\Gamma(2\times3)$, (e) kinetic energy $E(2\times3)$, Re=75,000

Figure 6. Vorticity distributions at t = 10, 14, 40, 60 for an impulsively started flow, Re = 1,000

Figure 7. Vorticity distributions at t = 10, 14, 40, 60 for a stratified flow, Re = 1,000, λ = 0.1

Figure 5 Streamfunction contours at t = 10, 14, 40, 60 for an unstratified flow, Re = 1,000

Figure 9. Streamfunction contours at t = 10, 14, 40, 60 for a stratified flow, Re = 1,000, λ = 0.1

Figure 10. Density departure contours at t = 2, 10, 40, 60 for a stratified flow, Re = 1000, N = 0.1